RSC Advances

PAPER

View Article Online
View Journal | View Issue

Cite this: *RSC Adv.*, 2020, **10**, 26588

Phase identification of vanadium oxide thin films prepared by atomic layer deposition using X-ray absorption spectroscopy

Yejin Kim,[a] Gwang Yeom Song,[b] Raju Nandi,[b] Jae Yu Cho,[b] Jaeyeong Heo *[b] and Deok-Yong Cho *[a]

Received 16th May 2020
Accepted 10th July 2020

DOI: 10.1039/d0ra04384b

rsc.li/rsc-advances

The chemical and local structures of vanadium oxide (VO_x) thin films prepared by atomic layer deposition (ALD) were investigated by soft X-ray absorption spectroscopy. It is shown that the as-deposited film was a mixture of VO_2 and V_2O_5 in disordered form, while the chemistry changed significantly after heat treatment, subject to the different gas environment. Forming gas (95% N_2 + 5% H_2) annealing resulted in a VO_2 composition, consisting mostly of the VO_2 (B) phase with small amount of the VO_2 (M) phase, whereas O_2 annealing resulted in the V_2O_5 phase. An X-ray circular magnetic dichroism study further revealed the absence of ferromagnetic ordering, confirming the absence of oxygen vacancies despite the reduction of V ions in VO_2 (V^{4+}) with respect to the precursor used in the ALD (V^{5+}). This implies that the prevalence of VO_2 in the ALD films cannot be attributed to a simple oxygen-deficiency-related reduction scheme but should be explained by the metastability of the local VO_2 structures.

Introduction

Transition metal oxides (TMOs) are being extensively studied for various applications in catalysis, electronics, and sensors.[1–3] Among these functional oxides, earth abundant vanadium oxides (VO_x) have garnered increasing attention due to their multiple oxidation states and various local structures, including octahedral, tetrahedral, triclinic, pentagonal bipyramids, and square pyramids.[4–6] VO_x exhibit remarkable interactions with ions and molecules, superior catalytic activity, suitable intercalation/deintercalation, and strong electron–electron correlations owing to their partially occupied d orbitals, which empower their utilization in a wide range of technological applications.[5,7–9]

Although research has mainly focused on VO_2 and V_2O_5 for numerous applications, including lithium ion batteries, gas sensors, fiber optic devices, actuators, data storage devices, switches, smart radiators, and thermochromic smart windows,[3,4,10–13] other vanadium oxides with stable stoichiometric and sub-stoichiometric phases have also displayed promising electrochemical properties.[14,15] Since the chemical and physical properties of VO_x vary substantially with the oxidation state of the vanadium cations, it is important to synthesize VO_x thin films with proper stoichiometry for their intended application.

Several thin film growth techniques, such as molecular beam epitaxy,[16] sputtering,[17] pulsed laser deposition,[18] electrodeposition, chemical vapor deposition,[19] and atomic layer deposition (ALD)[4] have been used to deposit VO_x thin films with different stoichiometries. ALD is a proven, extraordinarily controllable thin film deposition technique with great features, including atomically precise film thicknesses due to self-limiting reactions, uniform and conformal growth over large areas as well as over three-dimensional structures, pinhole free morphologies, and high reproducibility.[4,20,21] With the ALD process, VO_x thin films have been grown using different metal, metal–organic, and metal–halide precursors as the source material for vanadium and H_2O, H_2O_2, O_3, molecular O_2, and O_2 plasma as the oxidizing reactant.[4,14,17,22–24] Among these, vanadyl triisopropoxide (VTIP; V^{5+}) is the most popular vanadium precursor used for the ALD growth process.[4] Conventional ALD-grown VO_x thin films are amorphous in nature,[25,26] except for limited cases where crystalline films were successfully obtained.[4,22,27] Meanwhile, postdeposition annealing (PDA) in an appropriate ambient condition has been used to obtain single phase crystalline films.[4,26,28]

In an earlier work we reported the transformation of ALD-grown amorphous VO_x films into crystalline VO_2 and V_2O_5 by annealing in forming gas (FG; 95% N_2 + 5% H_2) and O_2, respectively, and their electrochemical and metal–insulator transition properties were investigated.[29] However, a detailed investigation of the local atomic structure was not undertaken to evaluate the formation of vanadium oxides with phase purity

[a]*IPIT, Department of Physics, Jeonbuk National University, Jeonju 54896, Korea. E-mail: zax@jbnu.ac.kr*

[b]*Department of Materials Science and Engineering, Optoelectronics Convergence Research Center, Chonnam National University, Gwangju 61186, Republic of Korea. E-mail: jheo@jnu.ac.kr*

and appropriate stoichiometry. Structural characterizations of the ALD VO_x films in previous reports used conventional X-ray diffraction (XRD).[4,30,31] VO_x systems, including VO_2 and V_2O_5, have distinct crystal structures depending on the stoichiometry,[11,30,32] and, furthermore, in the case of VO_2, there exist various phases, including A, B, M, and R, that possess distinct crystal structures as well.[32]

However, in the oxides prepared by ALD, certain residue, such as carbonates, or slightly nonstoichiometric regions often remain due to an insufficient purging time,[4,31] thus hindering the uniform long-range ordering of the atoms. In this case, the signals from the less crystalline or defective regions might not be captured evenly. This could hinder the accurate assessment of the mechanism by which the VO_2 phases (V^{4+}) are stabilized in the ALD films made from the VTIP (V^{5+}) precursor. Therefore, in this work, an alternative method, X-ray absorption spectroscopy (XAS) was employed to examine the chemical and structural properties of atoms regardless of the microstructural ordering.

XAS can provide information on the chemistry and local structure of each atomic species, which are averaged within the area of the beam spot (larger than 10 × 10 μm). In contrast to XRD, which reflects the crystal structures of long-range-ordered phases only, XAS can reveal not only the well-ordered structures but also the less-ordered or amorphous structures, so that a complete assessment of the VO_x phases in the grown films can be accomplished. In addition, by using circularly polarized X-rays with a tunable external magnetic field (B), the difference between the spectra measured under opposite B directions (called X-ray magnetic circular dichroism, XMCD) can probe for possible ferromagnetic ordering. There have been reports on a weak ferromagnetism in VO_2 (ref. 33) or V_2O_5 (ref. 34) films, which most plausibly originates from remnant V d electrons due to oxygen deficiency.[34,35] By using the V L-edge XMCD, the magnetic moment of V ions (not O or other impurities) can be obtained exclusively because XAS at the photon energies of the V L-edge dictates that the signals must be from the V ions. Thus, XMCD can measure the oxygen deficiency of the ALD VO_x films qualitatively, free from the effects of other impurities. Therefore, in this work, XAS (and XMCD) was performed on the ALD VO_x films to identify their averaged chemistry and local structures.

Experimental

Ten nanometer thick VO_x thin films were deposited on a Si substrate in a laminar-flow-type thermal ALD reactor (Atomic Classic, CN1, Korea) at a substrate temperature of 135 °C. VTIP (EG Chemical, Korea) and deionized water were used as the precursor and reactant, respectively. One ALD sequence was as follows: VTIP pulse (2 s), VTIP purge (15 s), H_2O pulse (5 s), and H_2O purge (20 s). More details of the growth process are described elsewhere.[29] The as-deposited films were then annealed at 500 °C for 1 h in an FG (95% N_2 + 5% H_2) or O_2 atmosphere in a box furnace (Hantech, C-A14P, Korea).

Soft XAS at V L- and O K-edges were performed at the 2A beamline at the Pohang Light Source. The direction of the incident X-rays was normal to the sample plane and a circular polarization (99%) was used. The base pressure of the measurement chamber was ~5×10^{-9} torr. The XAS data were collected for the three samples first at the room temperature (RT, 27 °C) and later at an elevated temperature (87 °C) to scrutinize a possible temperature-dependent phase evolution. The heating process in the vacuum had negligible influence on the spectral lineshapes of the as-deposited and O_2-annealed samples, while it only slightly shifted the spectrum of the FG-annealed sample. Negligible chemical changes subject to heating under such a low pressure reflect utmost thermal stability in as-deposited VO_x and V_2O_5. For the XMCD measurements, the samples were rotated by 23° with respect to the incident X-rays, and an external magnetic field of $B = \pm 0.7$ T was applied parallel or antiparallel to the sample normal direction.

Results and discussion

Fig. 1 shows the V $L_{2,3}$- and O K-edge XAS spectra of the as-deposited, O_2-annealed, and FG-annealed samples. The lineshapes of the three spectra are very different from each other, reflecting distinct local structures near the V and O ions. Overall, the spectra can be split into three regions: V L_3-edge (515–521 eV, V $2p_{3/2} \rightarrow 3d$), V L_2-edge (521–529 eV, V $2p_{1/2} \rightarrow 3d$), and O K-edge (529–550 eV, O 1s → O 2p hybridized with V 3d or 4sp).[36] The lineshapes of the V L-edge regions are determined primarily by the electron–electron interactions within the photoexcited V ions (Slater integrals, 3d Coulomb repulsion U, 2p–3d interactions, *etc.*) as well as the interactions between V and the neighboring O ions (crystal field, hybridization, *etc.*).[37] Thus, the chemistry and local structures of V ions can be examined by analyzing the V L-edge features. In principle, the lineshapes of the V L_2-edge region should be similar to those of the V L_3-edge region except for a small contribution from the 3d spin–orbit coupling.[38] Thus, the difference in appearance between the L_3- and L_2-edge regions originates predominately from the difference in the lifetime-related broadening of

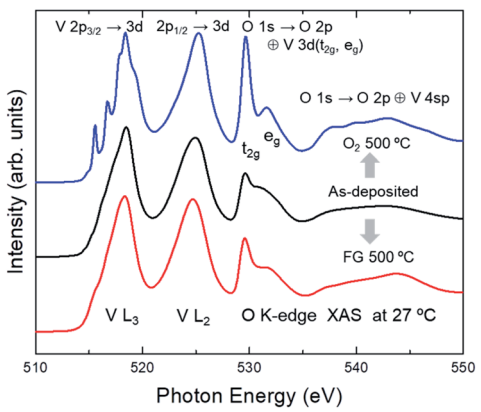

Fig. 1 V L- and O K-edge XAS spectra of as-deposited VO_x, as well as the FG- and O_2-annealed VO_x, measured at 27 °C. Fundamentally different lineshapes between the spectra clearly show the evolution of local structures from the annealing process.

features.[39] A detailed assessment of the V L-edge features is provided in subsequent figures.

In most of the 3d TMOs, such as TiO_x, FeO_x, or CoO_x,[40–42] the average valence of the TM ions can be roughly estimated by the energy of the most intense peak in the TM L_3- or L_2-edge spectrum. The energy of the most intense peak for the as-deposited VO_x is 518.4 eV, which is the same as that of V_2O_5, as shown in Fig. 2b. Thus, it is expected that the average valence of V ions should be close to +5. However, the energy of the most intense peak for VO_2 (V^{4+}), shown in Fig. 3, is also similar to that of V_2O_5, although there exists some variance in the peak energies among the polymorphs.[7] Therefore, unlike most of the other 3d TM oxides, it is difficult to determine from the L_3/L_2-edge peak positions whether annealing alters the average valences in the VO_x samples.

Meanwhile, the O K-edge region reflects mainly the unoccupied O 2p states that are hybridized with the V 3d (529–535 eV) or 4sp (535–550 eV) states, which are almost free from the effects of the core hole in the photoexcited final state.[37] The peak area of each feature in the O K-edge region reflects the number of unoccupied levels of the V 3d sub-states (t_{2g} or e_g in the octahedral point group notation) multiplied by the strength of the V 3d–O 2p orbital hybridizations. It is clearly seen that the intensities of the peaks near 529.5 eV for the three samples are different from each other. This suggests the number of unoccupied V 3d states is different among the samples, *i.e.*, the chemical formula of the VO_x varies subject to the annealing itself or the gas environment during annealing. This manifests the possibility of tuning the composition of ALD VO_x *via* the PDA process.[29]

To scrutinize the chemistry and local structures of the VO_x, the spectra taken at two different temperatures (RT and 87 °C) are displayed in Fig. 2 and 3. Fig. 2a and b show the spectra of the as-deposited and O_2-annealed VO_x, respectively. For the as-deposited sample, the lineshapes of the spectra are overall much broader than those for the O_2-annealed one. This is probably due to the significant structural disorders in the as-deposited VO_x, which is supported by the lack of prominent peaks in the XRD data.[29] Additionally, the intensities of the first peaks in the O K-edge region, which is related to the V 3d (t_{2g}) states, are weaker than those for the O_2-annealed (Fig. 2b) or FG-annealed sample (Fig. 1). This can also be attributed to the lower crystallinity of the as-deposited sample.

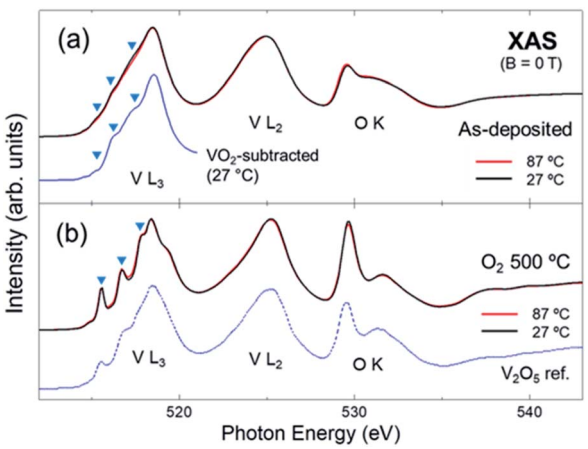

Fig. 2 Spectra of the (a) as-deposited and (b) O_2-annealed VO_x measured at 27 and 87 °C. The spectrum of V_2O_5 from ref. 8 is included for comparison. The results indicate that the local structure of as-deposited VO_x is a mixture of VO_2 (overall lineshape) and V_2O_5 (triangles), while that of the O_2-annealed VO_x is predominantly V_2O_5, regardless of the measurement temperature.

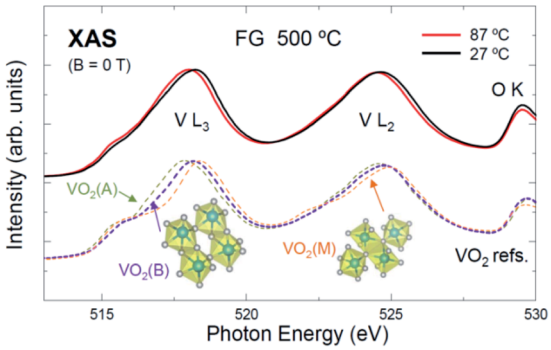

Fig. 3 Spectra of FG-annealed VO_x taken at 27 and 87 °C, and spectra of references VO_2(A), VO_2(B), and VO_2(M).[7,8] The local structure of FG-annealed VO_x is likely a combination of the VO_2(B) and VO_2(M) phases. The temperature evolution can be a signature of the transition from an insulator to a metallic phase, or a slight reduction of the V^{4+} ion due to vacuum heating (*i.e.*, $VO_{2-\delta}$) during the measurement.

Despite the significant structural disorder, the chemical states of the V and O ions in the as-deposited sample are most likely mixtures of those of the two annealed samples. As shown in Fig. 1, the overall lineshape of the spectrum of the as-deposited sample is nearly similar to the FG-annealed sample, and the small features in the L_3-edge spectra, highlighted by triangles in Fig. 2a, are coincident with those of the O_2-annealed sample. For clarity, the spectrum of the as-deposited film (27 °C) is displayed additionally in Fig. 2a after subtracting a half intensity of the VO_2 spectrum (in Fig. 3) so that the VO_2-subtracted spectrum would highlight the composition other than VO_2. Overall peak features in the difference spectrum are similar to those of the V_2O_5 spectra (Fig. 2b) manifesting substantial contribution of disordered V_2O_5 in the as-deposited film. The coexistence of two difference phases is reasonable in that the poor crystallinity or amorphous mixed state can evolve into a pure crystalline phase (for instance, either VO_2 or V_2O_5) subject to the thermodynamic equilibrium with the gas environment during annealing. Interestingly, the spectra of the as-deposited sample taken at both temperatures are very similar to each other. This implies that the evolution in the chemistry and local structure of the as-deposited VO_x was negligible even after the vacuum heating to 87 °C. Therefore, it can be concluded that the ALD VO_x is resistant to moderate heat, even though it is in a mixed phase.

For comparison, the spectrum of α-V_2O_5 powder from ref. 8 is included in Fig. 2b. The spectra of the O_2-annealed sample have very similar lineshapes to that of the V_2O_5 powder (but with considerably enhanced experimental energy resolution), indicating that the composition of the film is indeed α-V_2O_5.

The temperature dependence (RT *vs.* 87 °C) is negligible, suggesting a good thermal stability of the V_2O_5 film.

Fig. 3 shows the spectra of the FG-annealed sample taken at RT and 87 °C. For comparison, the spectra of the VO_2 polymorphs (VO_2 A, B, and M phases) taken from ref. 7 and 8 are included in the figure. The spectra at both temperatures are similar to those of the VO_2 phases while they are very different from that of V_2O_5 (see Fig. 2b). Additionally, the peak near 529.5 eV is weaker than that of V_2O_5 (V^{5+}; d^0), indicating a smaller number of the unoccupied t_{2g} levels. These findings suggest that the FG-annealed VO_x is VO_2 (V^{4+}; d^1). The lineshape of the spectra are most similar to that of VO_2(B), reflecting the dominance of the VO_2(B) phase. However, it is difficult to discern whether small amounts of the other phases (A or M) were incorporated or not.

The dominance of VO_2(B) appears inconsistent with a recent report,[29] in which XRD data showed the existence of crystalline VO_2(M), and its insulator–metal transition, when voltage was applied. However, XAS reflects the averaged local structure regardless of the crystallinity of each microstate, whereas XRD only shows the structure the crystallites. Thus, the RT data may contain a small contribution from the VO_2(M) phase as well. Schematics of the (local) structures of VO_2(B) and VO_2(M)[43,44] are included in Fig. 3.

Interestingly, the V L-edge peaks in the high temperature (87 °C) data show a rather rigid redshift by ~0.1 eV compared to those in the RT data. This could be attributed to a slight reduction of V^{4+} ions (*i.e.*, $VO_{2-\delta}$) that preserves the local structure of VO_2(B). Such partial reduction could occur during the vacuum heating; the pressure of the measurement chamber was $\sim 5 \times 10^{-9}$ torr, and the duration for the vacuum heating (87 °C) was approximately 1 h. Alternatively, the redshift could be attributed to the phase transformation of the B or M phase to a metallic rhombohedral phase [VO_2(R)].[45] This is reasonable in that d orbitals in a metallic state would spread toward the bandgap, which can in principle lead to a redshift of the unoccupied states. On the other hand, the O K-edge peak (for instance, at 529.5 eV) did not suffer such a shift because the chemistry of O^{2-} would not be affected noticeably by either the O deficiency or metallicity. Therefore, it can be concluded that both mechanisms (reduction and insulator-to-metal transition) can account for the temperature dependence.

It is noteworthy that the ALD film in the as-deposited state was prepared from a VTIP source, in which the valence of V ions is +5. In contrast, the averaged valence of V ions in the as-deposited sample is between +4 (VO_2) and +5 (V_2O_5), indicating that the V ions are reduced compared to those in the source. Also, FG annealing involves an additional reduction of V ions by the partial release of O atoms. Indeed, as shown in Fig. 3, the V valence of the FG-annealed sample is +4 (VO_2). Thus, it is reasonable to assume that the as-deposited or FG-annealed samples would bear significant oxygen deficiencies (y) based on the V_2O_5 (V^{5+}) stoichiometry (*e.g.*, V_2O_{5-2y}). However, this is not the case for the ALD VO_x films, primarily owing to the existence of metastable VO_2 phases.

Fig. 4 shows the XAS and XMCD spectra of as-deposited and FG-annealed samples taken with a magnetic field of $B = \pm 0.7$ T. The XMCD signals [(B = +0.7 T)–(B = −0.7 T)] show no noticeable features except for noise, even when they are magnified by 1000 times, conclusively proving that there is no ferromagnetic ordering of d electrons in the V ions in both samples. The absence of V d magnetism in either the as-deposited (VO_2 + V_2O_5) or FG-annealed (VO_2) film rules out the possibility of a ferromagnetic ordering of itinerant electrons,[34,46] as in dilute magnetic semiconductors,[47,48] because of the negligible carrier concentrations below the detection limit (here, on the order of 0.1% of the d electron number). If a substantial number of oxygen vacancies were created while preserving the V_2O_5 local structure in the as-deposited VO_x or after FG annealing, it must leave d electrons on V ions, serving as the source of possible inter-site spin interactions. Therefore, the films cannot be regarded as intermediate defective systems, such as $VO_{2-\delta}$ or V_2O_{5-y}, but as a stable composite of stoichiometric VO_2 and V_2O_5 (in the as-deposited sample) and a VO_2 (B + M) phase (in the FG-annealed sample). This implies that the prevalence of V^{4+} (VO_2) in the two samples, being different from V^{5+} in the precursor, originates from the stability of the VO_2 local structures, not the oxygen vacancy itself.

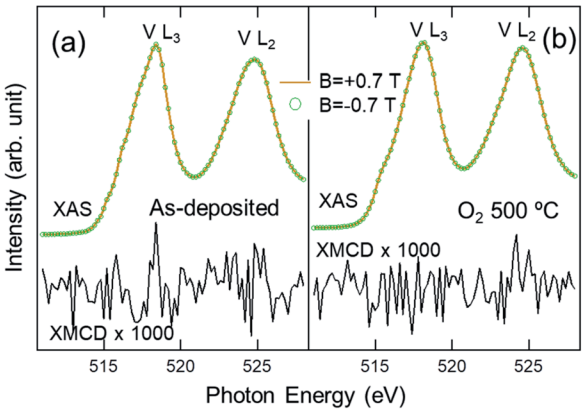

Fig. 4 XAS spectra taken at RT with $B = \pm 0.7$ T and the XMCD spectra (B = +0.7 T)–(B = −0.7 T) for (a) as-deposited and (b) FG-annealed VO_x. The XMCD signals (magnified by 1000 times) show no noticeable features except for noise, suggesting the absence of oxygen vacancies in both samples.

Note that the results of the XAS analyses show that the chemistry and local structures of the ALD VO_x films can be tuned effectively by applying PDA under the appropriate gas environment, *i.e.*, the forming gas for VO_2 and the O_2 gas for V_2O_5. This confirms that ALD with a subsequent PDA process under a specific gas environment is a promising route to control the phases in VO_2 or V_2O_5 thin films.

Conclusions

In conclusion, soft XAS analyses on ALD VO_x films revealed that the films exhibit various local structural phases subject to the PDA process: (i) the film in the as-deposited state is a composite of disordered VO_2 + V_2O_5, and (ii) during FG annealing, it transforms into VO_2 with local structures of B or B + M phases, while (iii) during O_2 annealing, it transforms into V_2O_5. The XMCD results confirmed the absence of oxygen vacancies in the

ALD VO_x films, implying that the apparent reduction of V ions (V^{4+} in VO_2) from those in the precursor (V^{5+}) is not associated with the oxygen defects but is allowed by the stability of the local VO_2 structure itself.

Conflicts of interest

There are no conflicts to declare.

Acknowledgements

This work was supported by Basic Science Research Program (2018R1D1A1B07043427) and Priority Research Centers Program (2018R1A6A1A03024334) through the National Research Foundation of Korea (NRF) funded by the Ministry of Education of Korea.

References

1 C. Imberti, P. Zhang, H. Huang and P. J. Sadler, *Angew. Chem.*, 2020, **132**, 61–73.
2 K. S. Kumar, G. L. Prajapati, R. Dagar, M. Vagadia, D. S. Rana and M. Tonouchi, *Adv. Opt. Mater.*, 2019, 1900958.
3 A. Sawa, *Mater. Today*, 2008, **11**, 28–36.
4 V. Prasadam, N. Bahlawane, F. Mattelaer, G. Rampelberg, C. Detavernier, L. Fang, Y. Jiang, K. Martens, I. Parkin and I. Papakonstantinou, *Mater. Today Chem.*, 2019, **12**, 396–423.
5 Z. Shao, X. Cao, H. Luo and P. Jin, *NPG Asia Mater.*, 2018, **10**, 581–605.
6 P. Shvets, O. Dikaya, K. Maksimova and A. Goikhman, *J. Raman Spectrosc.*, 2019, **50**, 1226–1244.
7 S. Lee, T. L. Meyer, C. Sohn, D. Lee, J. Nichols, D. Lee, S. S. A. Seo, J. W. Freeland, T. W. Noh and H. N. Lee, *APL Mater.*, 2015, **3**, 126109.
8 W.-L. Jang, Y.-M. Lu, C.-L. Chen, Y.-R. Lu, C.-L. Dong, P.-H. Hsieh, W.-S. Hwang, J.-L. Chen, J.-M. Chen and T.-S. Chan, *Phys. Chem. Chem. Phys.*, 2014, **16**, 4699–4708.
9 M. Liu, B. Su, Y. Tang, X. Jiang and A. Yu, *Adv. Energy Mater.*, 2017, **7**, 1700885.
10 D. McNulty, D. N. Buckley and C. O'Dwyer, *J. Power Sources*, 2014, **267**, 831–873.
11 J. Nag and R. Haglund Jr, *J. Phys.: Condens. Matter*, 2008, **20**, 264016.
12 K. Schneider, M. Lubecka and A. Czapla, *Sens. Actuators, B*, 2016, **236**, 970–977.
13 W. Zeng, N. Chen and W. Xie, *CrystEngComm*, 2020, **22**, 851–869.
14 F. Mattelaer, K. Geryl, G. Rampelberg, T. Dobbelaere, J. Dendooven and C. Detavernier, *RSC Adv.*, 2016, **6**, 114658–114665.
15 M. S. Whittingham, *Chem. Rev.*, 2004, **104**, 4271–4302.
16 E. Freeman, A. Kar, N. Shukla, R. Misra, R. Engel-Herbert, D. Schlom, V. Gopalan, K. Rabe and S. Datta, *70th Device Research Conference*, 2012.
17 K. Zhang, M. Tangirala, D. Nminibapiel, V. Pallem, C. Dussarrat, W. Cao, H. Elsayed-Ali and H. Baumgart, *ECS Trans.*, 2013, **50**, 175–182.
18 D. Kim and H. Kwok, *Appl. Phys. Lett.*, 1994, **65**, 3188–3190.
19 L. Crociani, G. Carta, M. Natali, V. Rigato and G. Rossetto, *Chem. Vap. Deposition*, 2011, **17**, 6–8.
20 P. O. Oviroh, R. Akbarzadeh, D. Pan, R. A. M. Coetzee and T.-C. Jen, *Sci. Technol. Adv. Mater.*, 2019, **20**, 465–496.
21 H. H. Sønsteby, A. Yanguas-Gil and J. W. Elam, *J. Vac. Sci. Technol., A*, 2020, **38**, 020804.
22 P. Dagur, A. U. Mane and S. Shivashankar, *J. Cryst. Growth*, 2005, **275**, e1223–e1228.
23 E. Østreng, O. Nilsen and H. Fjellvåg, *J. Phys. Chem. C*, 2012, **116**, 19444–19450.
24 R. Zhao, Y. Gao, Z. Guo, Y. Su and X. Wang, *ACS Appl. Mater. Interfaces*, 2017, **9**, 1885–1890.
25 K. Le Van, H. Groult, A. Mantoux, L. Perrigaud, F. Lantelme, R. Lindström, R. Badour-Hadjean, S. Zanna and D. Lincot, *J. Power Sources*, 2006, **160**, 592–601.
26 T. Singh, S. Wang, N. Aslam, H. Zhang, S. Hoffmann-Eifert and S. Mathur, *Chem. Vap. Deposition*, 2014, **20**, 291–297.
27 X. Chen, E. Pomerantseva, P. Banerjee, K. Gregorczyk, R. Ghodssi and G. Rubloff, *Chem. Mater.*, 2012, **24**, 1255–1261.
28 A. P. Peter, K. Martens, G. Rampelberg, M. Toeller, J. M. Ablett, J. Meersschaut, D. Cuypers, A. Franquet, C. Detavernier and J. P. Rueff, *Adv. Funct. Mater.*, 2015, **25**, 679–686.
29 G. Y. Song, C. Oh, S. Sinha, J. Son and J. Heo, *ACS Appl. Mater. Interfaces*, 2017, **9**, 23909–23917.
30 A. C. Kozen, H. Joress, M. Currie, V. R. Anderson, C. R. Eddy Jr and V. D. Wheeler, *J. Phys. Chem. C*, 2017, **121**, 19341–19347.
31 M. S. Weimer, I. S. Kim, P. Guo, R. D. Schaller, A. B. Martinson and A. S. Hock, *Chem. Mater.*, 2017, **29**, 6238–6244.
32 S. Lee, I. N. Ivanov, J. K. Keum and H. N. Lee, *Sci. Rep.*, 2016, **6**, 19621.
33 T.-H. Yang, S. Nori, S. Mal and J. Narayan, *Acta Mater.*, 2011, **59**, 6362–6368.
34 Z. Xiao and G. Guo, *J. Chem. Phys.*, 2009, **130**, 214704.
35 R. Molaei, R. Bayati, S. Nori, D. Kumar, J. T. Prater and J. Narayan, *Appl. Phys. Lett.*, 2013, **103**, 252109.
36 M. Abbate, H. Pen, M. Czyżyk, F. De Groot, J. Fuggle, Y. Ma, C. Chen, F. Sette, A. Fujimori and Y. Ueda, *J. Electron Spectrosc. Relat. Phenom.*, 1993, **62**, 185–195.
37 F. De Groot and A. Kotani, *Core level spectroscopy of solids*, CRC Press, 2008.
38 G. Van der Laan and B. Thole, *Phys. Rev. Lett.*, 1988, **60**, 1977.
39 G. van der Laan and B. Thole, *Phys. Rev. B: Condens. Matter Mater. Phys.*, 1991, **43**, 13401.
40 G. Henderson, X. Liu and M. Fleet, *Phys. Chem. Miner.*, 2002, **29**, 32–42.
41 F. Jiménez-Villacorta, C. Prieto, Y. Huttel, N. Telling and G. van der Laan, *Phys. Rev. B: Condens. Matter Mater. Phys.*, 2011, **84**, 172404.
42 M. Merz, P. Nagel, C. Pinta, A. Samartsev, H. v. Löhneysen, M. Wissinger, S. Uebe, A. Assmann, D. Fuchs and S. Schuppler, *Phys. Rev. B: Condens. Matter Mater. Phys.*, 2010, **82**, 174416.

43 C. Leroux, G. Nihoul and G. Van Tendeloo, *Phys. Rev. B: Condens. Matter Mater. Phys.*, 1998, **57**, 5111.
44 M. Zayed, A. Elabbar and O. Yassin, *Phys. B*, 2020, **582**, 411887.
45 J. Laverock, L. Piper, A. Preston, B. Chen, J. McNulty, K. Smith, S. Kittiwatanakul, J. Lu, S. Wolf and P.-A. Glans, *Phys. Rev. B: Condens. Matter Mater. Phys.*, 2012, **85**, 081104.
46 D. Guo, C. Hu, Q. Yang, H. Hua, W. Li and C. Kong, *Mater. Res. Bull.*, 2014, **53**, 102–106.
47 T.-H. Yang, S. Nori, H. Zhou and J. Narayan, *Appl. Phys. Lett.*, 2009, **95**, 102506.
48 S. Nori, T.-H. Yang and J. Narayan, *JOM*, 2011, **63**, 29.